Fourier Based Imaging Method with Steered Plane Waves and Limited-Diffraction Array Beams

Jiqi Cheng and Jian-yu Lu, Department of Bioengineering, The University of Toledo, Toledo, OH 43606, USA, jilu@eng.utoledo.edu

***Abstract* – A high frame rate (HFR) imaging theory was developed based on limited diffraction beams in 1997 (up to 3750 three-dimensional (3D) volumes/s for a depth of 200 mm in biological soft tissues). In this paper, the theory is extended to include explicitly various transmission schemes such as multiple limited-diffraction array beams and steered plane waves. Computer simulations and *in vitro* and *in vivo* experiments were performed to verify the extended theory. Results show that the extended theory provides a continuous compromise between image quality and frame rate which is useful in clinic.**

Keywords-limited diffraction beams; Fourier method; ultrasound imaging; high frame rate imaging

I. INTRODUCTION

A two-dimensional (2D) and three-dimensional (3D) high frame rate imaging (HFR) method [1]-[2] was developed based on limited diffraction beams [3]-[4] by one of the authors (Lu) in 1997 and was noted as one of the predictions of the 21st century medical ultrasonics [5]. Furthermore, Lu has suggested using steered plane waves in transmissions to increase image field of view and reduce speckle noises (see P.840 and P.850 of [1], and P.85, 94 and Fig. 8 of [2]) [6]-[7] or using limited-diffraction array beams in transmission to increase field of view and spatial Fourier domain coverage to increase image resolution [1]-[2], [8]. Images constructed with different steering angles can be combined with a coherent (enhancing resolution) or incoherent superposition (reducing speckles) [1]-[2], [6]-[7]. To increase field of view, a method using a spherical wave transmission followed by Fourier transformation for image reconstruction has also been proposed [9].

In this paper, Lu has extended his theory of high frame rate imaging [1]-[2] to include explicitly various transmission schemes such as multiple limited-diffraction array beams [10] and steered plane waves. The extended theory includes Lu's earlier suggestions of using these transmission schemes [1]-[2], [8]. Lu has also proved that limited-diffraction array beam weightings of received echo signals over a 2D transducer aperture are the same as a 2D Fourier transform of these signals over the same aperture [11]. It is worth noting that with limited-diffraction array beam transmissions [1]-[2], [8], time or phase delays for signals applied to transducer elements are not necessary. This may allow using only single or a small number of transmitters for all transducer elements and thus may simplify imaging system greatly, especially in 3D imaging where over 10,000 transmitters may otherwise be needed.

To verify the extended theory, computer simulations, *in vitro* experiments on phantoms, and *in vivo* experiments on the human kidney and heart were performed. A high frame rate imaging system was used for the experiments [12]-[13]. Results show that the extended theory provides a continuous compromise between image quality and image frame rate, which is useful since in some applications such as imaging of liver and kidney where high frame rate imaging is not crucial, high quality images can be obtained at the expense of image frame rate.

II. THEORETICAL PRELIMINARY

Superposing X waves [3]-[4], one obtains limited diffraction array beams [10] in transmission (Φ^T_{Array}) and reception (Φ^R_{Array}), respectively [11]:

$$\begin{aligned}\Phi^T_{Array}(\vec{r}_0,t) &= \frac{1}{2\pi}\int_0^\infty A(k)e^{ik_{x_T}x_0+ik_{y_T}y_0+ik_{z_T}z_0}e^{-i\omega t}dk \\ &= \frac{1}{2\pi}\int_{-\infty}^\infty A(k)H(k)e^{ik_{x_T}x_0+ik_{y_T}y_0+ik_{z_T}z_0}e^{-i\omega t}dk\end{aligned} \quad (1)$$

and

$$\Phi^R_{Array}(\vec{r}_0,t) = \frac{1}{2\pi}\int_{-\infty}^\infty T(k)H(k)e^{ik_xx_0+ik_yy_0+ik_zz_0}e^{-i\omega t}dk\,, \quad (2)$$

where $\vec{K}^T=(k_{x_T},k_{y_T},k_{z_T})$ and $\vec{K}^R=(k_x,k_y,k_z)$ are transmission and reception wave vectors, respectively, $\vec{r}_0=(x_0,y_0,z_0)$ is a point in space, t is the time, $k=\omega/c$ is the wave number, where ω is the angular frequency and c is the speed of sound. $A(k)$ and $T(k)$ are the transmission and reception transfer functions, respectively, and $H(k)$ is the Heaviside step function [14].

Convolving (1) with (2) in terms of time and multiplying the result with an object function, $f(\vec{r}_0)$, and then integrating over the space $\vec{r}_0$, one obtains the echo signals from the object. Taking temporal Fourier transform of echo signals, one obtains a relationship between the Fourier transform of the echo signals in terms of time ($\tilde{R}$) and the 3D spatial Fourier transform of the object function (F):

$$\begin{aligned}\tilde{R}_{k_x+k_{x_T},k_y+k_{y_T},k_z+k_{z_T}}(\omega) &= \frac{A(k)T(k)H(k)}{c^2} \\ &\times F(k_x+k_{x_T},k_y+k_{y_T},k_z+k_{z_T})\,, \quad (3)\end{aligned}$$

or

$$F_{BL}(k_x^{'},k_y^{'},k_z^{'}) = c^2H(k)\tilde{R}_{k_x^{'},k_y^{'},k_z^{'}}(\omega)$$

This work was supported in part by a grant, HL60301, from the National Institute of Health of USA.

where $F_{BL} = A(k)T(k)F$ is a band-limited version of F, $H(k)$ is moved to the side of $\tilde{R}$ for convenience, and where

$$\begin{cases} k_x' = k_x + k_{x_T} \\ k_y' = k_y + k_{y_T} \\ k_z' = k_z + k_{z_T} = \sqrt{k^2 - k_x^2 - k_y^2} + \sqrt{k^2 - k_{x_T}^2 - k_{y_T}^2} \ge 0 \end{cases} . \quad (4)$$

It is easy to prove that $\tilde{R}$ in (3) is also a 2D spatial Fourier transform over the transducer surface, $\vec{r}_1 = (x_1, y_1, 0)$, and one-dimensional (1D) Fourier transform in terms of time for echo signals received by transducer elements (e.g., a 2D array transducer) [11].

Equations (1) to (4) are also suitable for 2D imaging by simply setting y, k_y, and k_{y_T} to zero. For simplicity, in the following, we will show 2D results only. From (4), one obtains inverse formulae for limited-diffraction array beam and steered plane wave transmissions, respectively (this allows fast Fourier transform (FFT) to be used in image reconstructions):

$$\begin{cases} k_x = k_x' - k_{x_T} \\ k = \dfrac{\sqrt{\left(k_z'^2 + k_{x_T}^2 - \left(k_x' - k_{x_T}\right)^2\right)^2 + 4k_z'^2\left(k_x' - k_{x_T}\right)^2}}{2k_z'} \end{cases}, \quad (5)$$

and

$$\begin{cases} k_x = k_x' - k\sin\zeta_T \\ k = \dfrac{k_z'^2 + k_x'^2}{2k_z'\cos\zeta_T + 2k_x'\sin\zeta_T} \end{cases} . \quad (6)$$

For limited-diffraction array beam transmissions, the parameter k_{x_T} is fixed for all k in each transmission. Both sine and cosine aperture weightings are applied to transducer surface for each fixed k_{x_T} ($0 \le k_{x_T} \le k_{x_T\_\max} = \pi/\Delta x_1$), where Δx_1 is the pitch (spacing between transducer elements). For multiple transmissions, k_{x_T} is equally spaced. For steered plane wave transmissions, the Axicon angle of the X wave [3]-[4], ζ_T, is fixed for all k in each transmission (ζ_T is also the steering angle). ζ_T is equally spaced between $\pm\pi/4$ for multiple transmissions. For conventional delay-and-sum (D&S) method, the following formula is used to obtain the evenly spaced sine of the steering angles:

$$\sin\theta_n = n(\lambda_0/2)/D, \quad n = 0, \pm1, \pm2, \cdots, \pm(N-1)/2, \quad (7)$$

where θ_n ($|\theta_n| \le \pi/4$) is the nth-steering angle, λ_0 is the center wavelength, D is the transducer aperture, and N is an integer.

III. Simulations and Experiments

The simulation algorithms are developed based on the impulse response methods [15]-[19]. A one-cycle sine wave pulse at the center frequency of the transducer is used to excite the transducer. The simulation results are shown in Figs. 2-4.

Results of *in vitro* experiments of phantoms are shown in Figs. 5-10. *In vivo* experiments of a human kidney and a heart are shown in Figs. 11 and 12, respectively.

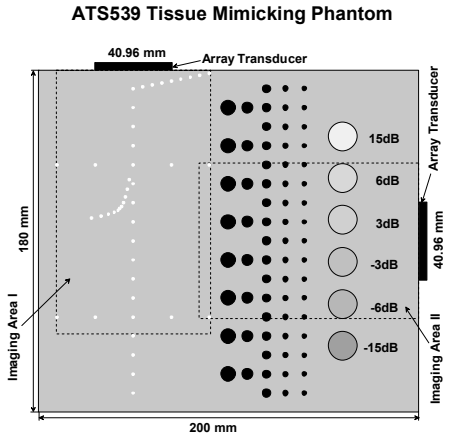

Figure 1. Structure and imaging areas of an ATS539 multipurpose tissue-mimicking phantom.

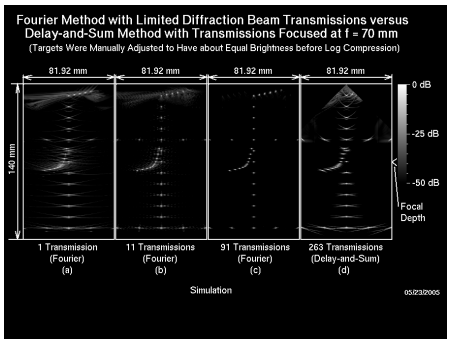

Figure 2. Simulated images according to the imaging Area I of the ATS539 phantom (see Fig. 1). Images are reconstructed with limited-diffraction array beam transmissions. Images are log-compressed at 50 dB. The transducer has 128 elements, 40.96 mm aperture, 0.32 mm pitch, 3.5 MHz center frequency, and 58% -6dB pulse-echo bandwidth. The area of each image panel is 81.92 x 140 mm. Images are obtained with (a) 1 (up to 5500 frames/s with 1540 m/s speed of sound), (b) 11 (up to 500 frames/s), and (c) 91 (up to 60 frames/s) transmissions, respectively. (d) Result obtained with the conventional delay-and-sum (D&S) method with a fixed transmission focal depth of 70 mm and with 263 transmissions (up to 21 frames/s).

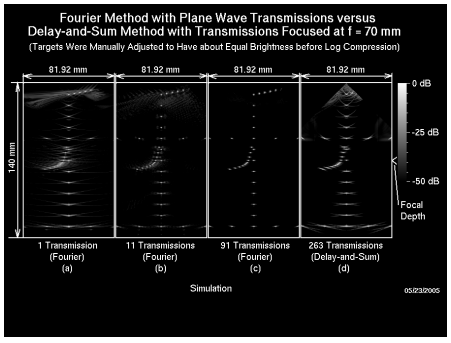

Figure 3. The same as Fig. 2 except that steered plane waves are used in transmissions, instead of limited-diffraction array beams.

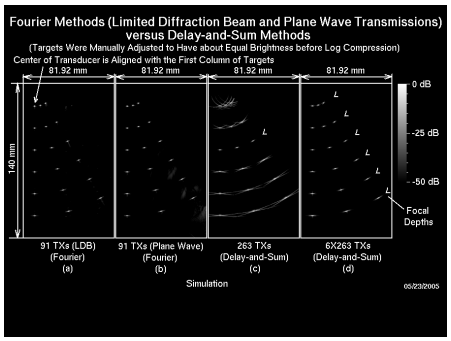

Figure 4. Simulated images for 18 point scatterers on three lines with 15 degrees between the lines. Six point scatterers are distributed evenly over each line with 20 mm spacing. The log compression, image panel size, and the parameters of the transducer are the same as those in Fig. 2. Image reconstructed with: (a) limited-diffraction array beam transmissions (91 transmissions up to 59 frames/s); (b) steered plane wave transmissions; (c) D&S method with a fixed focal depth at 60 mm (263 transmissions up to 20 frames/s); and (d) D&S method with a dynamically focused transmission synthesized using a montage process.

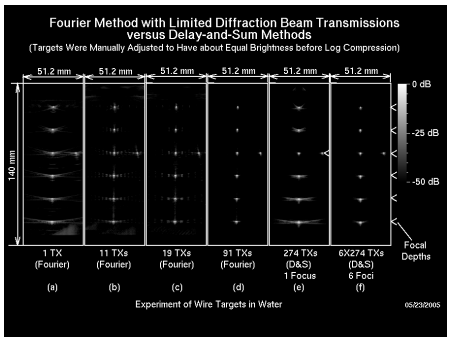

Figure 5. Experiment results of a wire phantom in water. Images are reconstructed with limited-diffraction array beam transmissions. There are 7 wires in total with 6 wires in a line and one wire on the third row 20 mm to the right of the line. The image panel size is 51.2 x 140 mm. The 6 wires are evenly distributed with 20 mm spacing. The log compression and the parameters of the transducer are the same as those in Fig. 2, except that the -6dB pulse-echo bandwidth of the transducer is about 50%, instead of 58%, of the center frequency. Images are obtained with (a) 1 (up to 5277 frames/s, with 1477.56 m/s speed of sound), (b) 11 (up to 479 frames/s), (c) 19 (up to 278 frames/s), and (d) 91 (up to 58 frames/s) transmissions, respectively. (e) Result obtained with the D&S method with a fixed transmission focal depth of 60 mm and with 274 transmissions (up to 19 frames/s); and (f) Result of the D&S method with a dynamically focused transmission synthesized with a montage process.

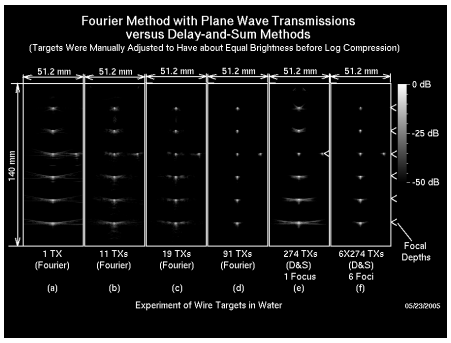

Figure 6. The same as Fig. 5 except that steered plane waves are used in transmissions instead of limited-diffraction array beams.

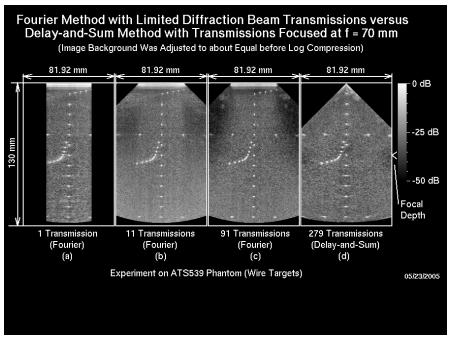

Figure 7. The same as Fig. 2 except that these are experiment results from a real ATS539 phantom on imaging Area I (see Fig. 1) using a real transducer. The speed of sound of the phantom is 1450 m/s and the -6dB pulse-echo bandwidth of the transducer is about 50% of the center frequency.

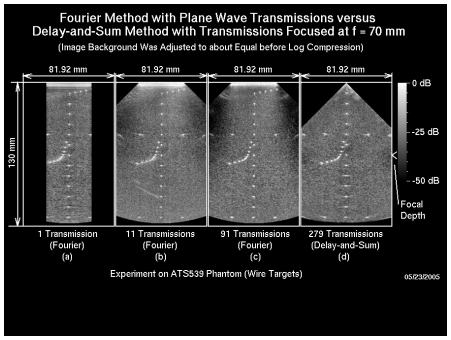

Figure 8. The same as Fig. 7 except that steered plane waves are used in transmissions instead of limited-diffraction array beams

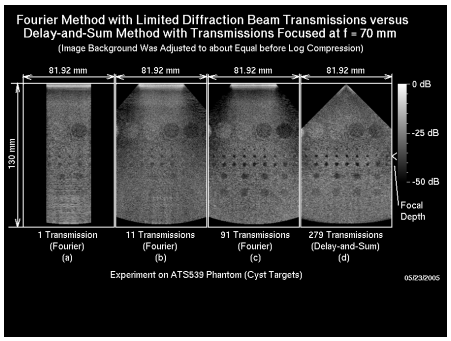

Figure 9. The same as Fig. 7 except that the imaging Area II of cystic objects of the ATS539 phantom (see Fig. 3) is used in the experiments.

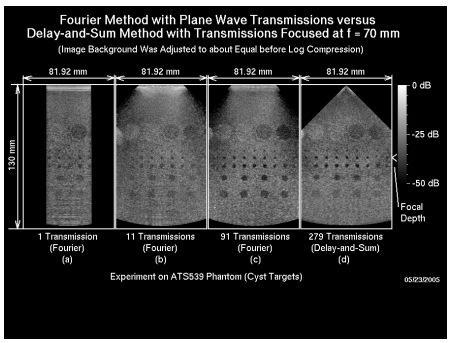

Figure 10. The same as Fig. 9 except that steered plane waves are used in transmissions instead of limited-diffraction array beams.

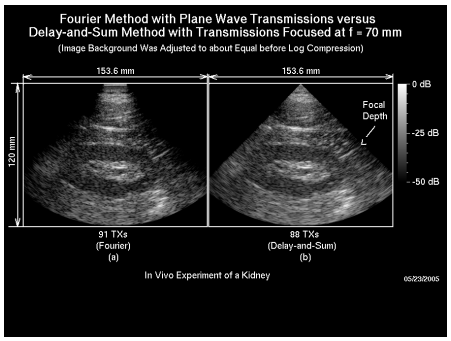

Figure 11. *In vivo* experiments of a right kidney of a volunteer. An Acuson V2 probe of 128 element, 2.5 MHz center frequency, 19.2 mm aperture, 0.15 mm pitch, and 14 mm elevation with 68 mm elevation focal depth is used. The depth of images is 120 mm. Data are acquired at the highest frame rate that the HFR system is allowed for the depth (187 μs between transmissions or 5348 frames/s for a speed of sound of 1540 m/s). (a) Image reconstructed with 91 steered plane wave transmissions (59 frames/s). (b) Image reconstructed with the D&S method with a fixed focal depth of 70 mm and 88 transmissions (61 frames/s).

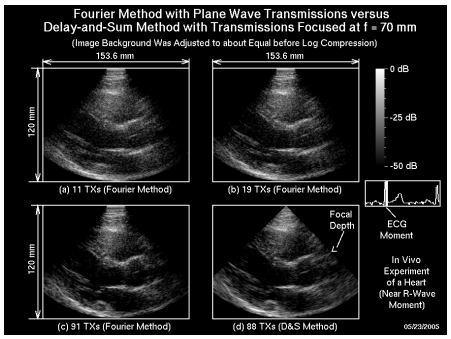

Figure 12. *In vivo* experiments of the heart of a volunteer. The transducer parameters, the depth of images, and the settings of the HFR imaging system are the same as those in Fig. 11. Data acquisition of the heart is triggered and synchronized by an electrocardiograph (ECG) signal to get images at the desired heart cycle moments (see the ECG display on the right hand side panel). Image reconstructed with (a) 11 (486 frames/s), (b) 19 (281 frames/s), and (c) 91 (59 frames/s) steered plane wave transmissions. (d) Image reconstructed with the D&S method with a fixed focal depth of 70 mm and 88 transmissions (61 frames/s).

IV. Conclusion

The high frame rate 2D and 3D imaging theory [1]-[2] has been extended to include explicitly various transmission schemes such as multiple limited-diffraction array beams and steered plane waves [11]. The function, $\tilde{R}$, in (3) has been shown by one of the authors (Lu) to be exactly the same as the spatial and temporal Fourier transform of the echo signals received with a 2D array transducer [11]. Computer simulations and *in vitro* and *in vivo* experiments are performed. Results show that the extended theory can be used to reconstruct images of a higher quality than those of the conventional D&S method of a synthesized dynamic transmission focusing using a montage process, which reduces image frame rate dramatically. Because FFT and limited-diffraction array beam transmissions can be used with the extended theory, imaging system may be greatly simplified.

Acknowledgments

The authors appreciate Mr. Jing Wang's help in the *in vivo* experiments. This work was supported in part by a grant HL 60301 from the National Institute of Health.

References

[1] Jian-yu Lu, "2D and 3D high frame rate imaging with limited diffraction beams," *IEEE Transactions on Ultrasonics, Ferroelectrics, and Frequency Control*, vol. 44, no. 4, pp. 839-856, July, 1997.

[2] Jian-yu Lu, "Experimental study of high frame rate imaging with limited diffraction beams," *IEEE Transactions on Ultrasonics, Ferroelectrics, and Frequency Control*, vol. 45, no. 1, pp. 84-97, January, 1998.

[3] Jian-yu Lu and J. F. Greenleaf, "Nondiffracting X waves - exact solutions to free-space scalar wave equation and their finite aperture realizations," *IEEE Transactions on Ultrasonics, Ferroelectrics, and Frequency Control*, vol. 39, no. 1, pp. 19-31, January, 1992.

[4] Jian-yu Lu and J. F. Greenleaf, "Experimental verification of nondiffracting X waves," *IEEE Transactions on Ultrasonics, Ferroelectrics, and Frequency Control*, vol. 39, no. 3, pp. 441-446, May, 1992.

[5] Glen Wade, "Human uses of ultrasound: ancient and modern," *Ultrasonics*, vol.38, pp.1-5 (2000).

[6] Jian-yu Lu, "Nonlinear processing for high frame rate imaging," *Journal of Ultrasound in Medicine*, vol. 18, no. 3 (Supplement), p. S50, March, 1999.

[7] Jian-yu Lu and Shiping He, "Increasing field of view of high frame rate ultrasonic imaging," *Journal of Acoustical Society of America*, vol. 107, no. 5, pt. 2, pp. 2779, May, 2000.

[8] Jian-yu Lu, "Transmit-receive dynamic focusing with limited diffraction beams," in *IEEE 1997 Ultrasonics Symposium Proceedings*, 97CH36118, vol. 2, pp. 1543-1546, 1997 (ISSN: 1051-0117).

[9] Hu Peng and Jian-yu Lu, "High frame rate 2D and 3D imaging with a curved or cylindrical array," in *IEEE 2002 Ultrasonics Symposium Proceedings* 02CH37388, vol. 2, pp. 1725-1728, 2002 (ISSN: 1051-0117).

[10] Jian-yu Lu, "Limited diffraction array beams," *International Journal of Imaging System and Technology*, vol. 8, no. 1, pp. 126-136, January, 1997 (ISSN: 0899-9457).

[11] Jiqi Cheng and Jian-yu Lu, " Extended high frame rate imaging method with limited-diffraction beams," *IEEE Transactions on Ultrasonics, Ferroelectrics, and Frequency Control* (submitted).

[12] Jian-yu Lu and John L. Waugaman, "Development of a linear power amplifier for high frame rate imaging system," in *IEEE 2004 Ultrasonics Symposium Proceedings*, 04CH37553C, vol. 2, pp. 1413-1416, 2004 (ISSN: 0-7803-8413-X).

[13] Jian-yu Lu, "A multimedia example," *IEEE Transactions on Ultrasonics, Ferroelectrics, and Frequency Control*, vol.50, no. 9, pp. 1078, September, 2003.

[14] R. Bracewell, *The Fourier Transform and its Applications*. New York: McGraw-Hill, 1965, Ch. 4 and 6.

[15] G. E. Tupholme, "Generation of acoustic pulses by baffled plane pistons," *Mathematika*, vol. 16, pp. 209-224, 1969.

[16] P. R. Stepanishen, "The time-dependent force and radiation impedance on a piston in a rigid infinite planar baffle," *J. Acoust. Soc. Am.*, vol.49, no. 3, pp. 841-849, 1971.

[17] G. R. Harris, "Review of transient field theory for a baffled planar piston," *J. Acoust. Soc. Am.*, vol. 70, pp. 1-20, 1981.

[18] J. A. Jensen and N. B. Svendsen, "Calculation of pressure fields from arbitrily shaped, apodized, and excited ultrasound transdcuers," *IEEE Trans. Ultrson., Ferroelect., Freq. Contr.*, vol. 39, no. 2, Mar, 1992.

[19] J. A. Jensen, "A new calculation procedure for spatial impulse responses in ultrasound," *J. Acoust. Soc. Am.*, vol.105, no. 6, pp. 3266-3274, 1999.